Single cell transcriptome analysis reveals disease-defining T cell subsets in the tumor microenvironment of classic Hodgkin lymphoma

Aoki, Tomohiro; Chong, Lauren C; Takata, Katsuyoshi; Milne, Katy; Hav, Monirath; Colombo, Anthony; Chavez, Elizabeth A; Nissen, Michael; Wang, Xuehai; Miyata-Takata, Tomoko

Published in:
Cancer discovery

DOI:
10.1158/2159-8290.CD-19-0680

Publication date:
2020

Single cell transcriptome analysis reveals disease-defining T cell subsets in the tumor microenvironment of classic Hodgkin lymphoma

Tomohiro Aoki[1,2,∞], Lauren C. Chong[1,∞], Katsuyoshi Takata[1], Katy Milne[3,4], Monirath Hav[5], Anthony Colombo[5], Elizabeth A. Chavez[1], Michael Nissen[6], Xuehai Wang[6], Tomoko Miyata-Takata[1], Vivian Lam[6], Elena Viganò[1,2], Bruce W. Woolcock[1], Adèle Telenius[1], Michael Y. Li[1,2], Shannon Healy[1], Chanel Ghesquiere[3,4], Daniel Kos[3,4], Talia Goodyear[3,4], Johanna Veldman[7], Allen W. Zhang[8, 9], Jubin Kim[6], Saeed Saberi[8], Jiarui Ding[8,10], Pedro Farinha[1], Andrew P. Weng[6], Kerry J. Savage[1], David W. Scott[1], Gerald Krystal[6], Brad H. Nelson[3,11], Anja Mottok[1,12], Akil Merchant[5], Sohrab P. Shah[2,8,9], and Christian Steidl[1,2,*]

[1] Centre for Lymphoid Cancer, British Columbia Cancer, Vancouver, BC, Canada
[2] Department of Pathology and Laboratory Medicine, University of British Columbia, Vancouver, BC, Canada
[3] Deeley Research Centre, British Columbia Cancer, Vancouver, BC, Canada
[4] Department of Biochemistry and Microbiology, University of Victoria, Victoria, BC, Canada
[5] Cedars-Sinai Medical Center, Los Angeles, California, USA
[6] Terry Fox Laboratory, British Columbia Cancer, Vancouver, BC, Canada
[7] Department of Pathology and Medical Biology, University Medical Center Groningen, University of Groningen, Groningen, The Netherlands
[8] Department of Molecular Oncology, British Columbia Cancer, Vancouver, BC, Canada
[9] Department of Epidemiology and Biostatistics, Memorial Sloan Kettering Cancer Center, New York, USA
[10] Broad Institute of MIT and Harvard, Cambridge, MA, USA
[11] Department of Biochemistry and Microbiology, and Department of Biology, University of Victoria, Victoria, BC, Canada
[12] Institute of Human Genetics, Ulm University and Ulm University Medical Center, Ulm, Germany
[∞] - equal contribution

***Corresponding Author:**
Christian Steidl, MD
Centre for Lymphoid Cancer, British Columbia Cancer, Vancouver, BC, Canada

675 West 10th Ave, Room 12-110, Vancouver, BC V5Z 1L3, Canada
E-mail: CSteidl@bccancer.bc.ca
Phone (office): 604-675-8046
FAX:604-675-8183

Running Title: Single cell characterization of Hodgkin lymphoma

Key words: Hodgkin lymphoma, single-cell sequencing, immune biology, tumor microenvironment, LAG3

COMPETING INTERESTS

C. Steidl reports receiving a commercial research grant from Bristol-Myers Squibb, Trillium Therapeutics, and is a consultant/advisory board member for Seattle Genetics, Curis, and Roche.

ABSTRACT

Hodgkin lymphoma (HL) is characterized by an extensively dominant tumor microenvironment (TME) composed of different types of non-cancerous immune cells with rare malignant cells. Characterization of the cellular components and their spatial relationship is crucial to understanding crosstalk and therapeutic targeting in the TME. We performed single-cell RNA sequencing of more than 127,000 cells from 22 HL tissue specimens and 5 reactive lymph nodes, profiling for the first time the phenotype of the HL-specific immune microenvironment at single-cell resolution. Single-cell expression profiling identified a novel HL-associated subset of T cells with prominent expression of the inhibitory receptor LAG3, and functional analyses established this $LAG3^+$ T cell population as a mediator of immunosuppression. Multiplexed spatial assessment of immune cells in the microenvironment also revealed increased $LAG3^+$ T cells in the direct vicinity of MHC class-II deficient tumor cells. Our findings provide novel insights into TME biology and suggest new approaches to immune checkpoint targeting in HL.

STATEMENT OF SIGNIFICANCE

We provide detailed functional and spatial characteristics of immune cells in cHL at single cell resolution. Specifically, we identified a Treg-like immunosuppressive subset of $LAG3^+$ T cells contributing to the immune escape phenotype. Our insights aid in the development of novel biomarkers and combination treatment strategies targeting immune checkpoints.

INTRODUCTION

Classic Hodgkin lymphoma (cHL) is the most common lymphoma subtype among adolescents and young adults(1). cHL is characterized by an extensive microenvironment composed of different types of non-cancerous normal immune cells, such as several types of T cells, B cells, eosinophils and macrophages, and a rare population (~1%) of clonal malignant Hodgkin and Reed-Sternberg (HRS) cells(1-3). While some findings support the concept that the HRS cells recruit these immune cells to form a tumor-supporting, regulatory tumor microenvironment (TME) with limited anti-tumor activity in cHL(4-6), the complex interactions between HRS cells and their TME remain only partially understood. A deeper understanding of this symbiotic cellular crosstalk ('ecosystem') may lead to the development of novel biomarkers and therapeutic approaches.

Immune checkpoint inhibitors, such as the programmed death 1 (PD-1) inhibitors nivolumab and pembrolizumab, have shown dramatic efficacy in relapsed or refractory cHL with an overall response rate (ORR) of 65-87%(7,8), and durable remissions of approximately 1.5 years(8), which compares very favorably to other agents in this setting(9). Although the emergence of novel drugs emphasizes the need for the identification of predictive biomarkers that can provide a rationale for treatment

selection, it remains unclear which cells are the most important targets of immune checkpoint inhibitors and which components are most relevant for the immune escape phenotype in cHL. Thus, further comprehensive investigations of this interaction are needed.

Previous studies have applied immunohistochemistry (IHC), microarray, cytometry by time-of-flight (CyTOF) and NanoString assays to characterize the immune phenotype of the TME in cHL, and have identified some important associations between the presence of certain immune cell types and clinical outcome(4,6,10). Although previous reports have described enrichment of $CD4^+$ T cells in the TME of cHL(10-12), their study scale has been limited and detailed co-expression patterns of important markers such as inhibitory receptors have not been examined.

Recently, the landscape of tumor infiltrating T cells has been assessed using single-cell transcriptome sequencing in several solid tumors, mostly of epithelial origin(13,14). These single-cell RNA sequencing (scRNA-seq) studies have revealed diverse immune phenotypes, such as cells exhibiting an exhaustion signature, as well as clonal expansion patterns of T cell lineages(14). However, such analyses are currently lacking in lymphomas, which differ from most solid cancers in that they are clonally derived from lymphocytes that professionally interact with other immune cells in the

ecosystem of the microenvironment.

In this study, we performed high dimensional and spatial profiling of immune cells in cHL using scRNA-seq of 127,786 cells, multicolor IHC and imaging mass cytometry (IMC). We identified unique regulatory T cell-like subset that expressed lymphocyte activation gene 3 ($LAG3^+$ T cells) in cHL and were mostly absent in normal reactive lymph nodes. $LAG3^+$ T cells were characterized by expression of interleukin-10 (IL-10) and transforming growth factor β (TGF-β), and we demonstrated an immuno-suppressive function of these cells. Further topological analysis revealed that HRS cells were closely surrounded by frequent $LAG3^+$ T cells in the subset of cHL patients with loss of Major histocompatibility class II (MHC-II) expression on tumor cells. Our data provide an unprecedented number of single-cell transcriptomes in combination with multiplexed spatial assessment, allowing us to decipher the unique immune cell architecture of the TME in cHL with implications for novel therapies, including rational combinations and predictive biomarker development.

RESULTS

The cHL-specific immune microenvironment at single-cell resolution

To characterize the transcriptional profile of immune cells in the TME of cHL, we performed scRNA-seq on single cell suspensions collected from lymph nodes of 22 cHL patients, including 12 of nodular sclerosis (NS) subtype, 9 of mixed cellularity (MC) subtype, and 1 of lymphocyte-rich (LR) subtype. We also sequenced reactive lymph nodes (RLN; n = 5) from healthy donors as normal controls (**Supplementary Tables 1 and 2**). Transcriptome data were obtained for a total of 127,786 sorted live cells, with a median of 1,203 genes detected per cell (**Supplementary Table 3**). To perform a systematic comparative analysis of the cHL TME and RLN, we merged the expression data from all cells (cHL and RLN) and performed batch correction and normalization. Removal of batch effects (caused by single cell isolation and library preparation in different experimental runs) resulted in improved mixing of cells across samples, as demonstrated by a significant increase in cell entropy (Wilcoxon-Mann-Whitney $p < 0.001$; **Supplementary Fig. 1A-B**).

Unsupervised clustering using PhenoGraph followed by visualization in t-SNE space(15,16) identified 22 expression-based cell clusters that were annotated and assigned to a cell type based on the expression of genes described in published

transcriptome data of sorted immune cells(17) and known canonical markers (**Fig. 1A; Supplementary Fig. 2A-E and 3**). These included 4 naïve T cell clusters, 2 $CD8^+$ T cell clusters, 6 $CD4^+$ T cell clusters, 7 B cell clusters, 1 macrophage cluster, 1 plasmacytoid dendric cell cluster and 1 progenitor cell cluster. We coud not observe HRS cell cluster may be due to limitation of microfluidics approach. While most immune cell phenotypes exhibited overlap between cHL and RLN as demonstrated by clusters containing a mixture of cell types, we observed an enrichment of cells from cHL in some specific cell clusters (**Fig. 1B**). Of interest, we found that all three regulatory T cell (Treg) clusters were quantitatively dominated by cells derived from the cHL samples with only a minor proportion originating from RLNs (**Fig. 1C**), and that the proportion of cells assigned to Treg clusters was significantly higher in cHL samples compared to RLN ($P = 0.0001$; t-test; **Fig. 1D**). The cluster containing the highest proportion of immune cells from cHL samples ("CD4-C5-Treg") also exhibited relatively high expression of LAG3 and CTLA4 (**Fig. 1A**). Conversely, clusters enriched in RLN were mostly B cell and $CD8^+$ T cell clusters (**Fig. 1C**). Further examination of the non-Treg $CD4^+$ T cell clusters revealed that they were primarily composed of type 2 T helper (Th2) cells, and that Th1 and Type 17 T helper (Th17) cells were also enriched in cHL samples compared to RLN (**Fig. 1E**). We also

181 performed differential expression analysis between cHL and RLN cells within each
182 cluster, and identified IL-32 as consistently upregulated in cHL T cells compared to
183 RLN T cells (**Supplementary Fig. 4**). IL-32 is a known pro-inflammatory cytokine that
184 can induce the production of other cytokines such as IL-6(18).
185
186 **EBV status affects the immune cell subset composition in cHL**
187 Thirty to 40% of cHL are associated with latent Epstein-Barr virus (EBV)
188 infection of the malignant HRS cells(19), and several reports indicate that EBV
189 infection can recruit specific Treg populations to the TME in cHL(20,21). To more
190 precisely define immune cell composition according to EBV status, we compared the
191 RNA-seq data of 5 EBV^+ *vs* 17 EBV^- cases (**Supplementary Fig. 5A**). The proportion
192 of $CD4^+$ T cells with a Th17 profile was significantly decreased in EBV^+ cHL (P =
193 0.004; t-test) (**Fig. 1F-G**). However, there was no significant difference between EBV^+
194 and EBV^- cases with respect to $CD8^+$ T cell or Treg proportions (**Fig. 1F;**
195 **Supplementary Fig. 5B**). Similarly, the cHL mixed cellularity (MC) subtype, which is
196 more commonly associated with EBV related cHL, was associated with a lower
197 proportion of Th17 polarized immune cells as compared to the nodular sclerosis (NS)
198 subtype (**Fig. 1H; Supplementary Fig. 5C**).

Single cell expression patterns of novel cHL-specific immune subsets

Our data demonstrated the preferential enrichment of Tregs in cHL as compared to RLN (**Fig. 1B and D**). Considering the importance of an immuno-suppressive microenvironment as a cancer hallmark, and its implications for biomarker development and targeted immunotherapy, we focused our analyses on the detailed characterization of Treg subsets. The most cHL-enriched Treg cluster, CD4-C5-Treg (**Fig. 1A**), was characterized by high expression of LAG3 in addition to common Treg markers such as IL2RA (CD25) and TNFRSF18 (GITR) (**Fig. 2A**). However, other canonical Treg markers such as FOXP3 were not co-expressed in this cluster, suggesting these cells may exhibit a type 1 regulatory (Tr1) T cell phenotype(20,22) (**Fig. 2B; Supplementary Fig. 6A**). To confirm the expression pattern of immune cells in cHL, we also assessed the expression of surface and intracellular markers in all cHL cases using multi-color IHC and IMC. The orthogonal data confirmed the inversely correlated expression pattern of LAG3 and FOXP3 on $CD4^+$ T cells at the protein level (**Supplementary Fig. 6B-C**).

Inhibitory receptor-mediated immune tolerance that can be hijacked by tumors has been a major target of cancer immunotherapy(23,24). To gain more insight into the

217 characteristics of inhibitory receptor expression in the TME of cHL, we explored
218 expression patterns among individual T cells. While LAG3-expressing cells were
219 mostly assigned to Treg clusters, PD-1-expressing cells were primarily assigned to
220 non-Treg $CD4^+$ T cell clusters (**Fig. 2C**). Interestingly, $CD8^+$ T cells, including CTLs,
221 are not the dominant population expressing PD-1 and LAG3 (**Fig. 2C-D**), indicating the
222 importance of the $CD4^+$ T cell population for immune checkpoint regulation in cHL.
223 Notably, the expression pattern of inhibitory receptors was variable among T cell
224 subsets (**Fig. 2E)**, suggesting a specific role of each inhibitory receptor in each T cell
225 subset in cHL. Analyzing co-expression patterns on the single cell level revealed that
226 the majority of $LAG3^+$ T cells co-expressed CTLA4 which is known as more universal
227 Treg marker, but not PD-1 (**Fig. 2F**). Similarly, most $PD\text{-}1^+$ T cells did not co-express
228 LAG3. CTLA-4 was also co-expressed by $FOXP3^+$ T cells (**Supplementary Fig. 6A**).
229 These co-expression patterns were validated using FCM (**Supplementary Fig. 7A-B**).
230 Interestingly, LAG3, TIGIT and PD-1 were not co-expressed by the majority of $CD8^+$ T
231 cells. Furthermore, although we observed a trend towards higher proportions of
232 non-TFH (Follicular helper T) $PD\text{-}1^+$ $CD4^+$ T cells in RLN samples, the proportion of
233 $LAG3^+$ cells was significantly higher in cHL, suggesting a unique role of $LAG3^+$ $CD4^+$
234 T cells in cHL pathogenesis (**Supplementary Fig. 7C)**.

To explore the functional role of LAG3$^+$ T cells, we next applied the diffusion map algorithm(25,26) with the aim of characterizing differentiation states among CD4$^+$ T cells (**Fig. 2G**). Most T cells were grouped by PhenoGraph cluster, and the first dimension showed a trajectory beginning with naïve T cells and ending with Tregs. LAG3$^+$ T cells were enriched at the far end of this dimension, which was correlated with genes representative of a terminal differentiation signature (**Methods; Supplementary Fig. 8A**). Consistent with a previous report that showed LAG3$^+$ T cells confer suppressive activity through their significantly reduced proliferation activity(27), LAG3$^+$ T cells were also located in the middle to negative end of the second dimension, which correlated with G2/M cell cycle and glycolysis signature genes (**Supplementary Fig. 8B**). Furthermore, the most positively correlated genes with dimension 1 were LAG3, LGMN and CTLA4, which are known markers of suppressive function in Tregs, indicating the suppressive signature of LAG3 in these T cells (**Supplementary Fig. 8C-D**).

cHL cell line supernatant can induce LAG3$^+$ T cells

To characterize the immunosuppressive signature of Tregs in cHL, we investigated the cytokine expression of LAG3$^+$ T cells. Among the CD4$^+$ cluster T cells,

LAG3$^+$ T cells had higher expression of immune-suppressive cytokines IL-10, TGF-β and IFN-γ compared to LAG3$^-$ T cells (**Fig. 3A**). These characteristics are consistent with the profile of type 1 regulatory T cells(28,29).

Taken together, our data consistently demonstrate a suppressive phenotype of LAG3$^+$ T cells in cHL. We hypothesized that cytokines or chemokines produced by HRS cells might influence the TME in cHL. Thus, we next assessed the effect of supernatant transfer of various lymphoma cell lines on the expansion of T cells *in vitro*. After 14 days of activation of T cells, flow cytometry analysis confirmed that CD4$^+$ CD25$^+$ T cells co-cultured with cHL cell line supernatant expressed significantly higher levels of LAG3 as compared to those co-cultured with diffuse large B-cell lymphoma (DLBCL) cell line supernatant or medium only (**Fig. 3B-C**). Luminex analysis revealed that the presence of cHL cell line supernatant resulted in enrichment of multiple cytokines and chemokines as compared to DLBCL cell lines, including TARC/CCL17, TGF-β, and IL-6, which are known enhancers of Treg migration and differentiation(30-38) (**Fig. 3D**). Consistent with scRNA-seq results, CD4$^+$ LAG3$^+$ T cells isolated by FACS secreted significantly higher amounts of IL-10 and TGF-β compared to CD4$^+$ LAG3$^-$ T cells (**Fig. 3E**). Notably, CD4$^+$ LAG3$^+$ T cells suppressed the proliferation of responder CD4$^+$ T cells when co-cultured *in vitro*,

confirming an immunosuppressive function of the LAG3$^+$ T cells (**Fig. 3F**).

Spatial assessment of LAG3$^+$ T cells and HRS cells

We next sought to understand the spatial relationship between LAG3$^+$ T cells and malignant HRS cells. IHC of all cases revealed that LAG3$^+$ T cells were enriched in the cHL TME compared to RLN, and in a subset of cHL cases HRS cells were closely surrounded by LAG3$^+$ T cells (**Fig. 4A**). Of note, our single cell analysis revealed that LAG3 expression was significantly higher in cases with MHC class II negative HRS cells (n = 6) as compared to those with MHC class II positive cHL cases (n = 16), but was not correlated with EBV status or histological subtype (**Fig. 4B; Supplementary Fig. 9A-C**). Strikingly, when examining cells within the CD4-C5-Treg cluster, LAG3 was identified as the most up-regulated gene in MHC class II negative cells compared to MHC class II positive cells (**Fig. 4C**). Characterization of immune markers using IHC showed not only a marked increase in LAG3$^+$ T cells, but also a decrease in FOXP3$^+$ T cells in MHC-II negative cases when compared to MHC-II positive cases (**Fig. 4D**). There was no difference in the proportion of CTLA4$^+$ CD4$^+$ T cells by MHC-II status, suggesting the LAG3$^+$ cells represent a distinct sub-population of the HL-specific CTLA4$^+$ cells previously reported(12) (**Supplementary Figure 9D**). To

validate these findings, we assessed the spatial relationship between HRS cells and LAG3$^+$ CD4$^+$ T cells using multicolor IHC (**Fig. 4E-G**). We confirmed that the density of LAG3$^+$ T cells in HRS-surrounding regions was significantly increased in MHC class II negative cases, but not correlated with either MHC class I status, pathological subtype or EBV status (**Fig. 4E; Supplementary Fig. 10A**). Similarly, the average nearest neighbor distance between CD30$^+$ cells (HRS cells) and their closest LAG3$^+$ T cell was significantly shorter in MHC class II negative cHL cases (**Fig. 4F)**. In contrast, the density of HRS-surrounding FOXP3$^+$ T cells was higher in cases with MHC class II positive HRS cells (**Fig. 4E; Supplementary Fig. 10B)**, and the nearest neighbor distance from HRS cells to FOXP3$^+$ cells was also shorter in these cases (**Fig. 4F; Supplementary Fig. 11A-B**).

To further investigate the spatial relationship between HRS cells and their surrounding cells, we next assessed the expression of surface and intracellular markers in all cHL study cases using IMC, which allows for simultaneous interrogation and visualization of 35 protein markers in the spatial context of the TME. Consistent with IHC analysis, IMC revealed that MHC class II negative cHL cases showed numerous LAG3$^+$ CD4$^+$ cells, with rare FOXP3$^+$ CD4$^+$ cells (**Fig. 5A; Supplementary Fig. 12A**). In contrast, MHC class II positive cases showed rare LAG3$^+$ CD4$^+$ T cells and abundant

FOXP3$^+$ CD4$^+$ T cells rosetting the HRS cells. We also confirmed the observed significantly shorter nearest neighbor distances between HRS cells and their closest LAG3$^+$ T cell in MHC class II negative cHL cases when compared to MHC class II positive cHL cases using IMC data (**Supplementary Fig. 12B-C**).

The number of LAG3$^+$ T cells in the tumor microenvironment is correlated with loss of MHC-II expression in a large validation cohort

We next validated our findings using IHC of an independent cohort of 166 patients uniformly treated with first-line ABVD (doxorubicin, bleomycin, vinblastine and dacarbazine) as described in Steidl et al(6) and investigated the potential prognostic value of the presence of LAG3$^+$ T cells. Consistent with the results from scRNA-seq, we found that the proportion of LAG3$^+$ T cells present in tumor tissue was significantly higher in cases with MHC class II negative HRS cells as compared to those with MHC class II positive HRS cells, but was not associated with EBV status (**Fig. 5B-C**). In addition, we observed a trend towards shortened disease-specific survival (DSS; P = 0.072) and overall survival (OS; P = 0.12) in patients with an increased number of LAG3$^+$ T cells (**Supplementary Fig. 13A-B**). Of note, a high proportion of LAG3$^+$ T cells (> 15%) and CD68$^+$ tumor-associated macrophages (≥ 5%)(6) were identified as

independent prognostic factors for DSS by multivariate Cox regression analysis (also considering MHC II expression and International Prognostic Score (IPS) as variables; (**Supplementary Fig. 13C**). In the absence of statistically significant outcome correlates in the present cohorts of pretreatment HL samples, we examined an independent cohort of patients with relapsed cHL uniformly treated with high dose chemotherapy followed by autologous stem cell transplantation (ASCT)(4). We similarly found that abundant $LAG3^+$ T cells were associated with unfavorable post-ASCT survival, although statistical significance was not reached, likely due to sample size (**Supplementary Fig. 13D**).

Cross-talk between HRS cells and $LAG3^+$ T cells in cHL

To investigate the role of HRS cells in their interaction with the cHL microenvironment, we next explored Affymetrix gene expression data generated from micro-dissected HRS cells of primary HL samples(39) (see **Supplementary Methods** for details). We validated the high expression level of the cytokines and chemokines that we observed in the *in vitro* Luminex assay (**Fig. 6A**. Notably, IL-6, which is a known promoter of Tr1 cell differentiation(38), was the only cytokine that showed significantly higher expression in MHC-II negative HRS cells compared to MHC-II

positive HRS cells. $CD4^+LAG3^+$ T cells were also induced by IL-6 *in vitro* (**Fig. 6B**), indicating that IL-6 might play a role in inducing $CD4^+LAG3^+$ T cells in cHL.

MHC-II is also a known LAG-3 ligand(40,41). To investigate the interaction between $LAG3^+$ T cells and MHC-II on HRS cells, we generated *CIITA* knockouts in the L-428 cHL cell line, as CIITA is the master regulator of MHC-II expression, and confirmed the MHC-II negative status of these *CIITA* knockout cells (**Supplementary Fig. 14A**). Next, we isolated $LAG3^+$ T cells induced from PBMC using L-428 supernatant transfer. In co-culture of these $LAG3^+$ T cells with either *CIITA* wild-type or knockout L-428 cells, we observed that LAG-3 expression was significantly decreased with MHC-II positive L-428, suggesting negative regulation of $LAG3^+$ T cell function through a direct MHC-II-LAG3 interaction (**Fig. 6C**). We also evaluated expression of cytokines, including IL-6 and TARC, from both *CIITA* wild-type and knockout L-428 cells, and observed no significant difference (**Supplementary Fig. 14B**). Taken together, these findings suggest that while IL-6 induces $LAG3^+$ T cells, MHC-II positivity actively depletes them, thus a mechanism for induction and persistence is present only in MHC-II negative tumors. We also investigated the expression of other LAG3 ligands on HRS cells according to MHC-II status in the Affymetrix dataset, and found that their expression was not significantly increased

relative to normal GCB cells (**Supplementary Fig. 14C**). In addition, there was no correlation between the expression level of LAG3 ligands according to MHC-II status, suggesting no direct interaction with these ligands in cHL.

T cells from cHL clinical samples are activated after removal of LAG3$^+$ T cells

To confirm the pathogenic role of LAG3$^+$ T cells in cHL clinical samples, we sorted both CD4$^+$ LAG3$^+$ CD25$^+$ T cells and remaining T cells from cell suspensions of 4 patients. We then co-cultured T cells with or without CD4$^+$ LAG3$^+$ CD25$^+$ T cells *in vitro*, and observed that proliferation was suppressed in the T cells co-cultured with the LAG3$^+$ population, while proliferation and expression of the intracellular cytokine, TNFα, were significantly increased in the population cultured without LAG3$^+$ cells (**Fig. 6D-E, Supplementary Fig. 15**). These results support an immunosuppressive function of CD4$^+$ LAG3$^+$ T cells in cHL clinical samples, providing preclinical rationale for targeting LAG3$^+$ T cells and their interactions to promote reactivation of T cells in a subset of patients.

Our results suggest a model in which the immunosuppressive microenvironment of MHC class II negative HRS cells (Type 1) is highly organized and in part induced by CD4$^+$ LAG3$^+$ T cells, which in turn are induced by cytokines and

chemokines produced by HRS cells (**Fig. 7**). Aggregating all of these results, we reason that cross-talk between LAG3$^+$ T cells and HRS cells may be an essential mechanism of immune escape in cHL, with potential implications for outcome prediction of differential checkpoint inhibitor therapy including response durability and overcoming resistance.

DISCUSSION

Using scRNA-seq and IMC at an unprecedented scale, we comprehensively characterized immune cell populations to generate an immune cell atlas of the TME in classic Hodgkin lymphoma at both the RNA and protein level. In addition to reproducing known TME characteristics in cHL at single cell resolution, such as a Treg/Th2-rich environment(10,11), a Th17-predominant profile in EBV$^+$ cHL(42), and a CTLA-4$^+$ PD1$^-$ T cell population(12), we also identified and characterized in detail novel cellular subpopulations, including immuno-suppressive LAG3$^+$ T cells(40) that are linked to unique pathologic and clinical parameters. Strikingly, Treg populations and the LAG3$^+$ T cell population in particular emerged as the most highly enriched and cHL-characteristic cellular component.

LAG3 is a selective marker of type 1 T regulatory (Tr1) cells, which in contrast to

natural Tregs derived from the thymus, are known as induced Tregs that exhibit strong immunosuppressive activity(20-22,27). Consistent with characteristics of Tr1 cells, the expression of the suppressive cytokines IL-10 and TGF-β(22,27), was very high in $LAG3^+$ T cells, whereas FOXP3 was not co-expressed in $LAG3^+$ T cells in our scRNA-seq and IMC data. Furthermore, $LAG3^+$ T cells demonstrated substantial suppressive activity *in vitro*, indicating an immunosuppressive role of these cells in the TME of cHL.

Unlike previous reports that found EBV infection increased Tr1-related gene expression including LAG3 in cHL(20), we identified a significant $LAG3^+$ Treg population regardless of EBV status by scRNA-seq, multi-color IHC, IMC, and single color IHC analyses in independent cohorts. However, our study revealed that $LAG3^+$ $CD4^+$ T cells were enriched in cases with MHC class II negative HRS cells. Interestingly, MHC class II deficiency was reported as a predictor of unfavorable outcome after PD-1 blockade(43). Our scRNA-seq data revealed that each T cell subset had a specific expression pattern of inhibitory receptors including PD-1 and LAG3. Most notably, the majority of $LAG3^+$ $CD4^+$ T cells did not co-express PD-1, and the absence of PD-1 has been reported to represent functionally active Tregs in solid cancer(44), indicating the potential of LAG3 as a separate and complementary

immunotherapeutic target in cHL. The FOXP3$^+$ Tregs that are enriched in MHC-II positive HRS cells in this study might be similar to the PD-1 negative FOXP3$^+$ Tregs previously reported(10).

MHC class II is one of the major ligands of LAG3(40,41) and we showed negative regulation of LAG3$^+$ T cell expression through MHC-II and LAG3 interaction using HL cell lines *in vitro*. These results are consistent with the patient data showing that LAG3$^+$ CD4$^+$ T cells were preferentially observed surrounding MHC class II negative HRS cells. Additionally, our *in vitro* co-culture findings suggest that cytokines and chemokines produced by HRS cells may be an important inducer of LAG3$^+$ CD4$^+$ T cells in the TME. In particular, re-analysis of expression on laser micro-dissected HRS cells revealed that MHC-II negative HRS cells had higher levels of IL-6, a cytokine known to induce Tr1 cells(38). Alternative ligands of LAG3 that mediate the immune suppressive function(45,46) might contribute to these interactions, although we did not observe any differences in their expression on HRS cells according to MHC-II status.

Our findings suggest that LAG3$^+$ T cells induced by cytokines and chemokines from HRS cells play an important role in substantial immunosuppressive activity in the TME of cHL. Importantly, LAG3 is a cancer immuno-therapeutic target in ongoing clinical trials in malignant lymphoma, including cHL (NCI trial ID 02061761), and we

showed the potential of removing the $LAG3^+$ population as a means of reactivating T cell activity. While currently our data do not demonstrate value of $LAG3^+$ T cells as a *prognostic* biomarker, and pending further studies in additional cohorts, it will be critical to evaluate the potential of $LAG3^+$ T cells as a *predictive* biomarker in the context of treatments targeting $LAG3^+$ T cells and their cellular interactions. In particular, ongoing trials of LAG3-targeting antibodies and antibody-drug conjugates against CTLA-4 or CD25 (which would target $LAG3^+$ cells among others) will allow this evaluation. Moreover, additional investigations into the biology of immune cell interactions, including $LAG3^+$ T cells and other immune cell types, may be beneficial for future therapeutic development of alternative checkpoint inhibitors.

In conclusion, our comprehensive analysis provides, for the first time, detailed functional and spatial characteristics of immune cells in the cHL microenvironment at single cell resolution. We identified unique expression signatures of TME cells, including $LAG3^+$ T cells, and our findings provide novel insights and texture to the central hypothesis of $CD4^+$ T cell mediated immune-suppressive activity in the pathogenesis of cHL. Importantly, our findings will facilitate a deeper understanding of the mechanisms underlying the immune escape phenotype in cHL, and aid in the development of novel biomarkers and treatment strategies.

METHODS

Detailed materials and methods are available in the Supplementary Data file.

Tissue samples

For single cell RNA sequencing, a total of 22 patients with histologically confirmed diagnostic (n = 21) or relapsed (n = 1) classic Hodgkin Lymphoma (cHL) and reactive lymphoid hyperplasia (but no evidence of malignant disease or systemic autoimmune disease) (n = 5) were included in this study. Patients were selected based on the availability of tissue that had been mechanically dissociated and cryopreserved as cell suspensions following diagnostic lymph node biopsy from British Columbia (BC) Cancer. Patient characteristics are summarized in Supplementary Table 1 and 2.

The independent validation cohort consisted of 166 cHL patients uniformly treated with ABVD at BC Cancer between 1994 and 2007 from the cohort described in Steidl et al(6). This cohort was derived from a population-based registry (Centre for Lymphoid Cancer database, BC Cancer Agency), enriched for treatment failure. The median follow-up time for living patients was 4.1 years (range: 0.5 to 24.4 years). The relapse cohort consisted of 55 relapsed or refractory cHL patients uniformly treated with high dose chemotherapy and ASCT at BC Cancer, from the cohort described in Chan et

al(4).

This study was reviewed and approved by the University of British Columbia-BC Cancer Agency Research Ethics Board (H14-02304), in accordance with the Declaration of Helsinki. We obtained written informed consent from the patients or the need for consent was waived in the retrospective study.

Single cell RNA sequencing sample preparation

To identify live cells, we used DAPI (Sigma-Aldrich, St. Louis, MO) for live-dead discrimination. Cell suspensions from cHL tumors or reactive lymph node were rapidly defrosted at 37^{o}C, washed in 10ml of RPMI1640/10% fetal bovine serum (FBS) solution or RPMI1640/20% FBS solution containing DNase I (Millipore Sigma, Darmstadt, Germany) and washed in PBS. Cells were resuspended in PBC containing 3% FBS and stained with DAPI for 15 min at 4°C in the dark. Viable cells (DAPI negative) were sorted on a FACS ARIAIII or FACS Fusion (BD Biosciences) using an 85 µm nozzle (**Supplementary Fig. 16**). Sorted cells were collected in 0.5 ml of medium, centrifuged and diluted in 1x PBS with 0.04% bovine serum albumin (BSA). Cell number was determined using a Countess II Automated Cell Counter whenever possible.

487

488 **Library Preparation and single-cell RNA sequencing**

489 In total, 8,600 cells per sample were loaded into a Chromium Single Cell 3' Chip kit v2
490 (PN-120236) and processed according to the Chromium Single Cell 3' Reagent kit v2
491 User Guide. Libraries were constructed using the Single 3' Library and Gel Bead Kit v2
492 (PN-120237) and Chromium i7 Mulitiplex Kit v2 (PN-120236). Single cell libraries
493 from two samples were pooled and sequenced on one HiSeq 2500 125 base PET lane.
494 CellRanger software (v2.1.0; 10X Genomics) was used to demultiplex the raw data,
495 generate quality metrics, and generate per-gene count data for each cell.

496

497 **Normalization and batch correction**

498 Analysis and visualization of scRNA-seq data was performed in the R statistical
499 environment (v3.5.0). CellRanger count data from all cells (n = 131,151) were read into
500 a single 'SingleCellExperiment' object. Cells were filtered if they had ≥ 20% reads
501 aligning to mitochondrial genes, or if their total number of detected genes was ≥ 3
502 median absolute deviations from the sample median. This yielded a total of 127,786
503 cells for analysis. The scran package (v1.9.11) was used to quick cluster the cells and
504 compute cell-specific sum factors with the method described by Lun et al(47). (see

505 **Supplementary Methods** for details). The scater package (v1.8.0) was used to
506 log-normalize the count data using the cell-specific sum factors.

507 To remove batch effects resulting from different chips and library preparation,
508 the fast mutual nearest neighbors (MNN) batch correction technique in the scran
509 package was utilized, grouping cells by their chip and using the expression of genes
510 with positive biological components (see **Supplementary Methods** for details). This
511 produced a matrix of corrected low-dimensional component coordinates (d = 50) for
512 each cell, which was used as input for downstream analyses. Entropy of cell expression
513 before and after batch correction was assessed in R using the method described by Azizi
514 et al(13) (**Supplementary Fig. 1B; Supplementary Methods**).

515

516 **Clustering and annotation**

517 Unsupervised clustering was performed with the PhenoGraph algorithm(48), using the
518 first 10 MNN-corrected components as input. Clusters from PhenoGraph were manually
519 assigned to a cell type by comparing the mean expression of known markers across cells
520 in a cluster (see **Supplementary Methods** for details). For visualization purposes, tSNE
521 transformation was performed with the scater package using the first 10 MNN-corrected
522 components as input. All differential expression results were generated using the

findMarkers function of the scran package, which performs gene-wise t-tests between pairs of clusters, and adjusts for multiple testing with the Benjamini-Hochberg method. Diffusion map analysis(25) was performed using the algorithm implemented by the scater package (**Supplementary Methods**).

Multi-color IHC on TMA, scanning and image analysis

TMA slides were deparaffinized and incubated with each marker of interest (MHC class II, FOXP3, CD8, LAG3, CD4, CD30), followed by detection using Mach2 HRP and visualization using Opal fluorophores (**Supplementary Table 4**; see **Supplementary Methods** for details). Nuclei were visualized with DAPI staining. TMA slides were scanned using the Vectra multispectral imaging system (PerkinElmer, USA) following manufacturer's instructions to generate .im3 image cubes for downstream analysis. To analyze the spectra for all fluorophores included, inForm image analysis software (v2.4.4; PerkinElmer, USA) was used. Cells were first classified into tissue categories using DAPI and CD30 to identify $CD30^{+}$ $DAPI^{+}$, $CD30^{-}$ $DAPI^{+}$, and $CD30^{-}DAPI^{-}$ areas via manual circling and training (**Supplementary Fig. 17**). The $CD30^{+}$ $DAPI^{+}$ regions were considered to be HRS-surrounding regions. Cells were then phenotyped as

positive or negative for each of the six markers (MHC class II, FOXP3, CD8, LAG3, CD4, CD30). Data were merged in R by X-Y coordinates so that each cell could be assessed for all markers simultaneously. Nearest neighbor analysis was performed with the spatstat R package (v1.58-2).

Imaging mass cytometry (IMC)

IMC was performed on a 5μm section of the same TMA described above. The section was baked at 60°C for 90 min on a hot plate, de-waxed for 20 min in xylene and rehydrated in a graded series of alcohol (100%, 95%, 80% and 70%) for 5 min each. Heat-induced antigen retrieval was conducted on a hot plate at 95°C in Tris-EDTA buffer at pH 9 for 30 min. After blocking with 3% BSA in PBS for 45 min, the section was incubated overnight at 4C with a cocktail of 35 antibodies tagged with rare lanthanide isotopes (**Supplementary Table 5**). The section was counterstained the next day for 40 min with iridium (Ir) and 3 min with ruthenium tetroxide (RuO4) as described in Catena et al(49). Slides were imaged using the Fluidigm Hyperion IMC system with a 1μm laser ablation spot size and frequency of 100-200Hz. A tissue area of 1000μm^2 per sample was ablated and imaged. Duplicate cores of the same samples

were ablated when morphologic heterogeneity was identified a priori on H&E. IMCTools (https://github.com/BodenmillerGroup/imctools) was used in conjunction with CellProfiler (v2.2.0) to segment images and identify cell objects (see **Supplementary Methods** for details).

Cell lines

The cHL cell lines KMH2, L428 and L-1236 were obtained from the German Collection of Microorganisms and Cell Cultures (DSMZ; http://www. dsmz.de/) between 2007 and 2010, and were used for experiments within 20 passages. Cultures were grown according to the standard conditions. Human DLBCL cell lines Karpas-422 were purchased from DSMZ, and maintained in RPMI1640 (Life Technologies) containing 20% FBS. The cell line OCI-Ly1 was obtained from Dr. L. Staudt (NIH) in 2009 and maintained in RPMI1640 (Life Technologies) containing 10% FBS. All cell lines were confirmed negative for *Mycoplasma* prior to culture using the Venor^{TM} GeM Mycoplasma Detection Kit, PCR-based (Sigma-Aldrich, MP0025). All cell lines were authenticated using short tandem repeat profiling.

574 **Cell isolation and purification of human T cells**

575 We purified $CD4^+$ and $CD8^+$ T lymphocytes from peripheral blood mononuclear cells
576 (PBMCs) (see **Supplementary Methods** for details). Isolated $CD4^+$ and $CD8^+$ T cells
577 were incubated in either supernatants from cHL cell lines (L-1236, L-428, KM-H2) or
578 diffuse large B-cell lymphoma cell lines (OCI-Ly1 and Karpas-422) or culture medium.
579 At the end of day 14, we washed and analyzed the T cells using flow cytometry for
580 characterization. We purified $CD4^+$ $LAG3^+$ T-cells and $CD4^+$ $LAG3^-$ T-cells by flow
581 sorting on a FACS Fusion (BD Biosciences) using a 85μm nozzle.
582

583 **Flow cytometry**

584 To characterize T cells *in vitro*, we stained cells with a panel of antibodies including
585 CD3, CD4, CD8 and LAG3 (see **Supplementary Methods** for details), and assessed
586 them using flow cytometry (LSRFortessa or FACSymphony, BD, Franklin Lakes, NJ,
587 USA). Flow cytometry data were analyzed using FlowJo software (v10.2; TreeStar,
588 Ashland, OR, USA) (**Supplementary Fig. 18**). Statistical analyses were performed
589 using GraphPad Prism Version 7 (GraphPad Software Inc., La Jolla, CA).
590

591 ***In vitro* suppression assay**

To evaluate the suppressive activity of $LAG3^+$ T cells, we stained $CD4^+$ T cells (responder cells) with proliferation dye (VPD450; BD Biosciences or Cell Trace Violet Cell proliferation kit; Thermofisher) and activated them using soluble monoclonal antibodies to CD3 and CD28 in PRIME XV T cell CDM medium or CD3/CD28 Beads (Thermo Fisher). We added purified $CD4^+$ $LAG3^+$ T cells induced by cHL cell line supernatant transfer, or purified from cell suspensions of cHL clinical samples (suppressor cells) at a ratio of 1:1. We calculated the percentage of divided responder T cells by gating on $CD4^+$ cells and T cell proliferation was determined based on proliferation dye dilution using flow cytometry (LSRFortessa and FACSymphony, BD, Franklin Lakes, NJ, USA).

Cytokine and chemokine detection

Cytokines and chemokines were measured by ELISA and custom Bio-Plex assays (see **Supplementary Methods** for details).

Generation of *CIITA* knock-out cells

608 L-428 cell lines were transduced with lentivirus expressing guide sequence against
609 *CIITA* to generate *CIITA* knock-out cells which abrogate the expression of MHC class II
610 (**Supplementary Fig. 19A-B**; see **Supplementary Methods** for details). MHC class II
611 expression was evaluated by staining the cells with FITC-HLA DR/DP/DQ antibody
612 (1:100, BD Biosciences #555558) and analyzed using the BD LSRFortessa^{TM}.
613 Subsequently, *CIITA* knock-out cells were sorted by mCherry^{+}, HLA DR^{-}/DP^{-}/DQ^{-},
614 DAPI^{-} using the BD FACSAria^{TM} Fusion sorter.

615

616 ***In vitro* HRS cells and T cell co-culture assay**

617 We purified CD4^{+} LAG3^{+} T cells from HLA-class-II matched (to L-428) PBMC as
618 described above. CD4^{+} LAG3^{+} T cells were co-cultured with either *CIITA* wild-type or
619 *CIITA* KO L-428 at 2:1 ratio in a 96 well plate.

620

621 **Survival analysis**

622 Overall survival (OS, death from any cause), disease specific survival (DSS, the time
623 from initial diagnosis to death from lymphoma or its treatment, with data for patients

624 who died of unrelated causes censored at the time of death) and post-BMT failure free
625 survival (post-BMT-FFS, time from ASCT treatment to cHL progression, or death from
626 cHL) were analyzed using the Kaplan-Meier method and results were compared using
627 the log rank test. Univariate and multivariate Cox regression analyses were performed
628 to assess the effects of prognostic factors. Survival analyses were performed in the R
629 statistical environment (v3.5.2).
630
631 **Statistical results & visualization**
632 All t-tests reported are two-sided Student's t-tests, and P-values < 0.05 were considered
633 to be statistically significant. In all boxplots, boxes represent the interquartile range with
634 a horizontal line indicating the median value. Whiskers extend to the farthest data point
635 within a maximum of 1.5 × the interquartile range, and colored dots represent outliers.
636
637 **Data availability**
638 Single cell RNA-seq BAM files (generated with CellRanger v2.1.0) are deposited in
639 EGA (EGAS00001004085) and are available by request. The figures associated with
640 the above raw datasets are Fig. 1-4 and Supplementary Fig. 1-10.
641

642 **Code availability**

643 Scripts used for data analysis are available upon request.

644

ACKNOWLEDGEMENTS

This study was funded by a research grant from the CCSRI and a Paul Allen Distinguished Investigator award (Frontiers Group) (C. Steidl). This study was also supported by a Program Project Grant from the Terry Fox Research Institute (C. Steidl, Grant No. 1061), Genome Canada, Genome British Columbia, CIHR, and the British Columbia Cancer Foundation (BCCF). T.A. was supported by fellowship from Japanese Society for The Promotion of Science and the Uehara Memorial Foundation. T.A. received research funding support from The Kanae Foundation for the Promotion of Medical Science. E.V. is supported by a Michael Smith Foundation for Health Research trainee award.

AUTHORS' CONTRIBUTIONS

Study design: T.A., L.C., A.M., S.P.S. and C.S.; Writing: T.A., L.C. and C.S.; Manuscript review: K.T., A.M., K.M., M.H., A.C., E.C., T.M-T., V.L., A.W.Z., A.P.W., K.J.S., D.W.S., G.K., B.N., A.M. and S.P.S.; Data interpretation: T.A., L.C., K.T., M.H., A.C. and C.S.; *In vitro* experiments: T.A., E.V., B.W.W., A.T., S.H., M.Y.L., X.W., M.N., J.K. and V.L.; Data analysis: T.A., L.C., M.H., A.C. and K.M.; Single cell processing: E.C.; IHC work: K.T., T.M-T., K.M., P.F., C.G., D.K. and T.G.;

663 Pathological review: K.T., T.M-T. and P.F.; Case identification: T.A., X.W. and A.M.;

664 IMC work: M.H. and A.C.; Supervision: A.P.W., K.J.S., D.W.S., G.K., B.N., A.M.,

665 S.P.S. and C.S.

666

667

668

669

REFERENCES

1. Swerdlow SH, Campo E, Harris NL, Jaffe ES, Pileri SA, Stein H., *et al.* WHO Classification of Tumours of Haematopoietic and Lymphoid Tissues. Revised 4th ed. Lyon, France: International Agency for Research on Cancer (IARC). 2017.
2. Mottok A, Steidl C. Biology of classical Hodgkin lymphoma: implications for prognosis and novel therapies. Blood **2018**;131:1654-65
3. Aoki T, Steidl C. Novel Biomarker Approaches in Classic Hodgkin Lymphoma. Cancer J **2018**;24:206-14
4. Chan FC, Mottok A, Gerrie AS, Power M, Nijland M, Diepstra A, *et al.* Prognostic Model to Predict Post-Autologous Stem-Cell Transplantation Outcomes in Classical Hodgkin Lymphoma. J Clin Oncol **2017**;35:3722-33
5. Steidl C, Shah SP, Woolcock BW, Rui L, Kawahara M, Farinha P, *et al.* MHC class II transactivator CIITA is a recurrent gene fusion partner in lymphoid cancers. Nature **2011**;471:377-81
6. Steidl C, Lee T, Shah SP, Farinha P, Han G, Nayar T, *et al.* Tumor-associated macrophages and survival in classic Hodgkin's lymphoma. N Engl J Med **2010**;362:875-85
7. Chen R, Zinzani PL, Fanale MA, Armand P, Johnson NA, Brice P, *et al.* Phase II Study of the Efficacy and Safety of Pembrolizumab for Relapsed/Refractory Classic Hodgkin Lymphoma. J Clin Oncol **2017**;35:2125-32
8. Armand P, Engert A, Younes A, Fanale M, Santoro A, Zinzani PL, *et al.* Nivolumab for Relapsed/Refractory Classic Hodgkin Lymphoma After Failure of Autologous Hematopoietic Cell Transplantation: Extended Follow-Up of the Multicohort Single-Arm Phase II CheckMate 205 Trial. J Clin Oncol **2018**;36:1428-39
9. Younes A, Gopal AK, Smith SE, Ansell SM, Rosenblatt JD, Savage KJ, *et al.* Results of a pivotal phase II study of brentuximab vedotin for patients with relapsed or refractory Hodgkin's lymphoma. J Clin Oncol **2012**;30:2183-9
10. Cader FZ, Schackmann RCJ, Hu X, Wienand K, Redd R, Chapuy B, *et al.* Mass cytometry of Hodgkin lymphoma reveals a CD4(+) regulatory T-cell-rich and exhausted T-effector microenvironment. Blood **2018**;132:825-36

11. Greaves P, Clear A, Owen A, Iqbal S, Lee A, Matthews J, *et al.* Defining characteristics of classical Hodgkin lymphoma microenvironment T-helper cells. Blood **2013**;122:2856-63
12. Patel SS, Weirather JL, Lipschitz M, Lako A, Chen PH, Griffin GK, *et al.* The microenvironmental niche in classic Hodgkin lymphoma is enriched for CTLA-4- positive T-cells that are PD-1-negative. Blood **2019** Oct 10. E-pub ahead of print
13. Azizi E, Carr AJ, Plitas G, Cornish AE, Konopacki C, Prabhakaran S, *et al.* Single-Cell Map of Diverse Immune Phenotypes in the Breast Tumor Microenvironment. Cell **2018**;174:1293-308 e36
14. Han A, Glanville J, Hansmann L, Davis MM. Linking T-cell receptor sequence to functional phenotype at the single-cell level. Nat Biotechnol **2014**;32:684-92
15. Zilionis R, Nainys J, Veres A, Savova V, Zemmour D, Klein AM, *et al.* Single-cell barcoding and sequencing using droplet microfluidics. Nat Protoc **2017**;12:44-73
16. Klein AM, Mazutis L, Akartuna I, Tallapragada N, Veres A, Li V, *et al.* Droplet barcoding for single-cell transcriptomics applied to embryonic stem cells. Cell **2015**;161:1187-201
17. Novershtern N, Subramanian A, Lawton LN, Mak RH, Haining WN, McConkey ME, *et al.* Densely interconnected transcriptional circuits control cell states in human hematopoiesis. Cell **2011**;144:296-309
18. Netea MG, Azam T, Ferwerda G, Girardin SE, Walsh M, Park JS, *et al.* IL-32 synergizes with nucleotide oligomerization domain (NOD) 1 and NOD2 ligands for IL-1beta and IL-6 production through a caspase 1-dependent mechanism. Proc Natl Acad Sci U S A **2005**;102:16309-14
19. Schmitz R, Stanelle J, Hansmann ML, Kuppers R. Pathogenesis of classical and lymphocyte-predominant Hodgkin lymphoma. Annu Rev Pathol **2009**;4:151-74
20. Morales O, Mrizak D, Francois V, Mustapha R, Miroux C, Depil S, *et al.* Epstein-Barr virus infection induces an increase of T regulatory type 1 cells in Hodgkin lymphoma patients. Br J Haematol **2014**;166:875-90
21. Gandhi MK, Lambley E, Duraiswamy J, Dua U, Smith C, Elliott S, *et al.* Expression of LAG-3 by tumor-infiltrating lymphocytes is coincident with the suppression of latent membrane antigen-specific CD8+ T-cell function in Hodgkin lymphoma patients. Blood **2006**;108:2280-9

22. Gagliani N, Magnani CF, Huber S, Gianolini ME, Pala M, Licona-Limon P, *et al.* Coexpression of CD49b and LAG-3 identifies human and mouse T regulatory type 1 cells. Nat Med **2013**;19:739-46
23. Andrews LP, Marciscano AE, Drake CG, Vignali DA. LAG3 (CD223) as a cancer immunotherapy target. Immunol Rev **2017**;276:80-96
24. Tumeh PC, Harview CL, Yearley JH, Shintaku IP, Taylor EJ, Robert L, *et al.* PD-1 blockade induces responses by inhibiting adaptive immune resistance. Nature **2014**;515:568-71
25. Haghverdi L, Buettner F, Theis FJ. Diffusion maps for high-dimensional single-cell analysis of differentiation data. Bioinformatics **2015**;31:2989-98
26. Coifman RR, Lafon S, Lee AB, Maggioni M, Nadler B, Warner F, *et al.* Geometric diffusions as a tool for harmonic analysis and structure definition of data: diffusion maps. Proc Natl Acad Sci U S A **2005**;102:7426-31
27. Huang CT, Workman CJ, Flies D, Pan X, Marson AL, Zhou G, *et al.* Role of LAG-3 in regulatory T cells. Immunity **2004**;21:503-13
28. Bacchetta R, Sartirana C, Levings MK, Bordignon C, Narula S, Roncarolo MG. Growth and expansion of human T regulatory type 1 cells are independent from TCR activation but require exogenous cytokines. Eur J Immunol **2002**;32:2237-45
29. Groux H, O'Garra A, Bigler M, Rouleau M, Antonenko S, de Vries JE, *et al.* A CD4+ T-cell subset inhibits antigen-specific T-cell responses and prevents colitis. Nature **1997**;389:737-42
30. Skinnider BF, Mak TW. The role of cytokines in classical Hodgkin lymphoma. Blood **2002**;99:4283-97
31. Lin Y, Xu L, Jin H, Zhong Y, Di J, Lin QD. CXCL12 enhances exogenous CD4+CD25+ T cell migration and prevents embryo loss in non-obese diabetic mice. Fertil Steril **2009**;91:2687-96
32. McFadden C, Morgan R, Rahangdale S, Green D, Yamasaki H, Center D, *et al.* Preferential migration of T regulatory cells induced by IL-16. J Immunol **2007**;179:6439-45
33. Wang X, Lang M, Zhao T, Feng X, Zheng C, Huang C, *et al.* Cancer-FOXP3 directly activated CCL5 to recruit FOXP3(+)Treg cells in pancreatic ductal adenocarcinoma. Oncogene **2017**;36:3048-58

34. Pierini A, Strober W, Moffett C, Baker J, Nishikii H, Alvarez M, *et al.* TNF-alpha priming enhances CD4+FoxP3+ regulatory T-cell suppressive function in murine GVHD prevention and treatment. Blood **2016**;128:866-71
35. Tran DQ. TGF-beta: the sword, the wand, and the shield of FOXP3(+) regulatory T cells. J Mol Cell Biol **2012**;4:29-37
36. Gobert M, Treilleux I, Bendriss-Vermare N, Bachelot T, Goddard-Leon S, Arfi V, *et al.* Regulatory T cells recruited through CCL22/CCR4 are selectively activated in lymphoid infiltrates surrounding primary breast tumors and lead to an adverse clinical outcome. Cancer Res **2009**;69:2000-9
37. Mizukami Y, Kono K, Kawaguchi Y, Akaike H, Kamimura K, Sugai H, *et al.* CCL17 and CCL22 chemokines within tumor microenvironment are related to accumulation of Foxp3+ regulatory T cells in gastric cancer. Int J Cancer **2008**;122:2286-93
38. Jin JO, Han X, Yu Q. Interleukin-6 induces the generation of IL-10-producing Tr1 cells and suppresses autoimmune tissue inflammation. J Autoimmun **2013**;40:28-44
39. Steidl C, Diepstra A, Lee T, Chan FC, Farinha P, Tan K, *et al.* Gene expression profiling of microdissected Hodgkin Reed-Sternberg cells correlates with treatment outcome in classical Hodgkin lymphoma. Blood **2012**;120:3530-40
40. Huard B, Prigent P, Pages F, Bruniquel D, Triebel F. T cell major histocompatibility complex class II molecules down-regulate CD4+ T cell clone responses following LAG-3 binding. Eur J Immunol **1996**;26:1180-6
41. Baixeras E, Huard B, Miossec C, Jitsukawa S, Martin M, Hercend T, *et al.* Characterization of the lymphocyte activation gene 3-encoded protein. A new ligand for human leukocyte antigen class II antigens. J Exp Med **1992**;176:327-37
42. Duffield AS, Ascierto ML, Anders RA, Taube JM, Meeker AK, Chen S, *et al.* Th17 immune microenvironment in Epstein-Barr virus-negative Hodgkin lymphoma: implications for immunotherapy. Blood Adv **2017**;1:1324-34
43. Roemer MGM, Redd RA, Cader FZ, Pak CJ, Abdelrahman S, Ouyang J, *et al.* Major Histocompatibility Complex Class II and Programmed Death Ligand 1 Expression Predict Outcome After Programmed Death 1 Blockade in Classic Hodgkin Lymphoma. J Clin Oncol **2018**;36:942-50

802 44. Zhang B, Chikuma S, Hori S, Fagarasan S, Honjo T. Nonoverlapping roles of
803 PD-1 and FoxP3 in maintaining immune tolerance in a novel autoimmune
804 pancreatitis mouse model. Proc Natl Acad Sci U S A **2016**;113:8490-5
805 45. Wang J, Sanmamed MF, Datar I, Su TT, Ji L, Sun J, *et al.* Fibrinogen-like
806 Protein 1 Is a Major Immune Inhibitory Ligand of LAG-3. Cell
807 **2019**;176:334-47 e12
808 46. Xu F, Liu J, Liu D, Liu B, Wang M, Hu Z, *et al.* LSECtin expressed on
809 melanoma cells promotes tumor progression by inhibiting antitumor T-cell
810 responses. Cancer Res **2014**;74:3418-28
811 47. Lun AT, Bach K, Marioni JC. Pooling across cells to normalize single-cell RNA
812 sequencing data with many zero counts. Genome Biol **2016**;17:75
813 48. Levine JH, Simonds EF, Bendall SC, Davis KL, Amir el AD, Tadmor MD, *et al.*
814 Data-Driven Phenotypic Dissection of AML Reveals Progenitor-like Cells that
815 Correlate with Prognosis. Cell **2015**;162:184-97
816 49. Catena R, Montuenga LM, Bodenmiller B. Ruthenium counterstaining for
817 imaging mass cytometry. J Pathol **2018**;244:479-84

818

819

FIGURE LEGENDS

Figure 1. Immune cell atlas of the Hodgkin lymphoma microenvironment at single-cell resolution. Cells from 22 cHL and 5 RLN cases were clustered using the PhenoGraph algorithm to identify groups of cells with similar expression patterns. **A**, Heatmap summarizing mean expression (normalized and log-transformed) of selected canonical markers in each cluster. Data has been scaled row-wise for visualization. The covariate bar on the left side indicates the component associated with each gene, and black boxes highlight prominent expression of known subtype genes. **B**, Single-cell expression of all cells from cHL and RLN in tSNE space (first two dimensions). Cells are colored according to PhenoGraph cluster. Subsets of cells from cHL and RLN samples are shown on the same coordinates below, respectively. **C**, Proportion of cells in each cluster originating from cHL and RLN samples. Clusters labeled in red highlight Treg clusters. Dashed white line represents the proportion of RLN cells in the total population. **D**, The proportion of cells assigned to a given immune cell type (as determined by cluster) was calculated for each sample. Boxplots summarize the distribution of the proportions for all samples, grouped by tissue type (cHL or RLN). P-values calculated using a t-test are shown above, and demonstrate a significant expansion in the proportion of Tregs present in cHL compared to RLN. **E**, Proportion of

838 $CD4^+$ T cells (non-Treg) assigned to various subsets, calculated per sample and
839 summarized with boxplots (see Methods for definition of subtypes). **F-G**, Proportion of
840 immune cell types as in **D-E**, with samples separated according to EBV status (RLN not
841 included). **H,** Proportion of immune cell types as in **e**, with samples separated according
842 to histological subtype (RLN not included).
843

844 **Figure 2. Detailed characterization and co-expression patterns of regulatory T cells**
845 **in the tumor microenvironment of classic Hodgkin Lymphoma. A**, Violin plots
846 showing distribution of expression values (normalized log-transformed) for genes
847 associated with Treg function. Cells from three cluster types are included: $CD4^+$ T cells
848 (non-Treg) (CD4-C1-Helper, CD4-C2-Helper and CD4-C3-Helper), $LAG3^+$ Tregs
849 (CD4-C5-Treg) and other Tregs (CD4-C4-Treg and CD4-C6-Treg). **B**, The number of
850 individual cells co-expressing Treg markers LAG3 and FOXP3 in all Treg clusters. **C**,
851 Proportion of LAG3 and PDCD1 (PD-1) positive cells in each cluster. **D**, Proportion of
852 LAG3 and PD-1 positive cells in all Tregs, $CD4^+$ T cells (non-Tregs), and all $CD8^+$ T
853 cells. **E**, Heatmap showing mean expression of inhibitory receptors for cluster subsets.
854 Expression values have been scaled row-wise for visualization. **F**, UpSet plot showing

855 co-expression patterns of inhibitory receptors (LAG3, PD-1, TIGIT, TIM3 and CTLA4)
856 for individual cells in the LAG3$^+$ Treg cluster. **G**, Cellular trajectories were inferred
857 using diffusion map analysis of cells in all CD4$^+$ T cell clusters (cHL cells only).
858 Individual cells are shown in the first two resulting dimensions, and are colored
859 according to cluster (LAG3$^+$ Treg cluster is shown in bold). Axis labels indicate the
860 signature most correlated with each dimension (see Methods).
861
862 **Figure 3. An immune suppressive microenvironment is characteristic of cHL and**
863 **is associated with LAG3 positivity. A,** Density plots showing the expression of
864 suppressive cytokines for cells in the LAG3$^+$ Treg cluster (CD4-C5-Treg). Cells are
865 grouped by LAG3 positivity and P-values were calculated using t-tests. **B,**
866 Representative flow cytometric analysis of CD25 and LAG3 expression on T cells
867 isolated from PBMCs cultured with supernatant of cHL cell line, L-1236, or medium,
868 respectively. **C,** The proportion of LAG3$^+$ cells among CD4$^+$ T cells cultured with
869 supernatant of cHL cell lines (KM-H2, L-428 and L-1236), diffuse large B-cell
870 lymphoma (DLBCL) cell lines (OCI-Ly1 and Karpas-422) or medium only. Data are
871 shown as the mean±SEM (n = 3). *P $\leq$ 0.05; **P $\leq$ 0.01. **D,** The amount of cytokines
872 and chemokines in the supernatant of cHL cell lines and DLBCL cell lines by Luminex

873 analysis. Data are shown as the mean±SEM (n = 3). **E,** The amount of cytokines and
874 chemokines in the supernatant of FACS-sorted $CD4^+$ $LAG3^+$ cells and $CD4^+$ $LAG3^-$
875 cells by Luminex analysis. Data are shown as the mean±SEM (n = 4). **P ≤ 0.01, *P ≤
876 0.0001. **F**, (left) A representative experiment showing proliferation of $CD4^+$ responder
877 T cells alone (bottom), co-cultured with FACS-sorted $CD4^+$ LAG^- T cells (middle), or
878 co-cultured with FACS-sorted $CD4^+$ $LAG3^+$ T cells (top). (right) The percentage of
879 proliferating $CD4^+$ responder T cells in each co-culture condition, relative to the normal
880 proliferation rate (alone). Data are shown as the mean±SEM (n = 4). *P ≤ 0.05.

881

882 **Figure 4. Spatial distribution of Hodgkin and Reed-Sternberg cells and $LAG3^+$ T**
883 **cells in cHL tumors. A,** Representative LAG3 immunohistochemistry of cHL tumor
884 biopsies and a reactive lymph node (×400, CHL03 and CHL05). **B**, Boxplot showing
885 mean LAG3 expression of cells in the $LAG3^+$ Treg cluster separated by MHC class II
886 (MHC-II) status on HRS cells as determined by IHC (P = 0.0186; t-test). **C**, Volcano
887 plot showing differentially expressed genes between cells in the $LAG3^+$ Treg cluster
888 originating from MHC-II positive or negative cases. The top 5 genes by absolute log
889 fold-change in each direction are highlighted in red. The y-axis summarizes P-values

corrected for multiple testing using the Benjamini-Hochberg method. **D**, IHC staining for major immune cell markers in representative cases with either MHC-II positive HRS cells (left) or MHC-II negative (right) HRS cells (×400). **E**, Boxplot showing the density of $CD4^+$ $LAG3^+$ T cells (left) or $CD4^+$ $FOXP3^+$ (right) in the region surrounding $CD30^+$ cells (HRS) for each sample, separated by tissue type and MHC-II status on HRS cells (t-test; ns: $P > 0.05$, *: $P \leq 0.05$, ***: $P \leq 0.001$, ****: $P \leq 0.0001$). **F**, Average nearest neighbor (NN) distance from an HRS cell ($CD30^+$) to the closest $CD4^+$ $LAG3^+$ cell (left) or $CD4^+$ $FOXP3^+$ cell (right) was calculated per sample, and separated by MHC-II status on HRS cells. P-values were calculated using t-tests. **G**, Multicolor IF staining (CHL03 and CHL05) for CD30 (yellow), MHC-II (green), and LAG3 (magenta) shows localization of $LAG3^+$ $CD4^+$ T cells to the region surrounding HRS cells in cases with MHC-II negative HRS cells.

Figure 5. Co-expression patterns and localization of immune cells according to HRS MHC-II status, using imaging mass cytometry. A, A representative case with MHC-II negative cHL case (CHL5) shows numerous $LAG3^+$ $CD4^+$ T cells (i) and few $FOXP3^+$ $CD4^+$ T cells (ii), with the $LAG3^+$ cells rosetting the HRS cells (iii-iv). In contrast, a representative MHC-II positive cHL case (CHL3) shows rare $LAG3^+$ $CD4^+$

T cells (v) and abundant FOXP3$^+$ CD4$^+$ T cells (vi), the latter surrounding HRS cells (vii-viii). **B**, Comparison of the proportion of LAG3$^+$ cells by MHC-II status in a validation cohort.(6) P-values were calculated using t-tests. **C**, Comparison of the proportion of LAG3$^+$ cells by EBV status in a validation cohort.(6) P-values were calculated using t-tests.

Figure 6. Interactions of HRS cells and CD4$^+$ LAG3$^+$ T cells. A, The expression of cytokines and chemokines on micro-dissected HRS cells from primary HL samples (separated by MHC class II status) and germinal center cells from reactive tonsil (GCB) (t-test; ns: $P > 0.05$, *: $P \leq 0.05$, **: $P \leq 0.01$, ****: $P \leq 0.0001$). **B**, The proportion of LAG3$^+$ cells among CD4$^+$ T cells after co-culture with supernatant of cHL cell lines (L-1236), medium with IL-6, or medium only. Data are shown as the mean ± SEM (n = 4) (**: $P \leq 0.01$). **C,** (left) A representative experiment showing LAG3 expression of CD4$^+$LAG3$^+$ T cells (HLA-matched with L-428) after co-culture with either *CIITA* wild-type (Red) or *CIITA* KO L-428 (Blue). LAG3 expression on the T cells was significantly decreased after co-culture with MHC-II positive (*CIITA* KO) cells. (right) The percentage of highly-expressing LAG3$^+$ T cells after co-culture with L-428 *CIITA* variants (wild-type or knockout). Data are shown as the mean ± SEM (n = 3). *: P ≤

926 0.05. **D,** (left) A representative experiment showing proliferation of $CD4^+$ T cells sorted
927 from cHL clinical samples (red), and the same cells co-cultured with $CD4^+LAG3^+$
928 $CD25^+$T cells from cHL clinical samples (blue). (right) The percentage of proliferating
929 cells in each condition are shown as the mean ± SEM (n = 4). *: $P \leq 0.05$ (t-test). **E,** The
930 expression of TNFα in the populations described in **D** are shown as the mean ± SEM (n
931 = 3). *: $P \leq 0.05$ (t-test).
932
933 **Figure 7. A model of $LAG3^+$ T cell and HRS cell interactions in classic Hodgkin**
934 **lymphoma.**
935 Hypothetical model of $LAG3^+$ T cell and HRS cell interactions in cHL. MHC-II
936 negative HRS cells (Type 1) secrete cytokines that induce LAG3 in $CD4^+$ T cells. $CD4^+$
937 $LAG3^+$ T cells surround HRS cells and secrete suppressive cytokines. MHC-II positive
938 cells (Type 2) secrete a distinct set of cytokines that attract $FOXP3^+$ and Th17 cells.
939

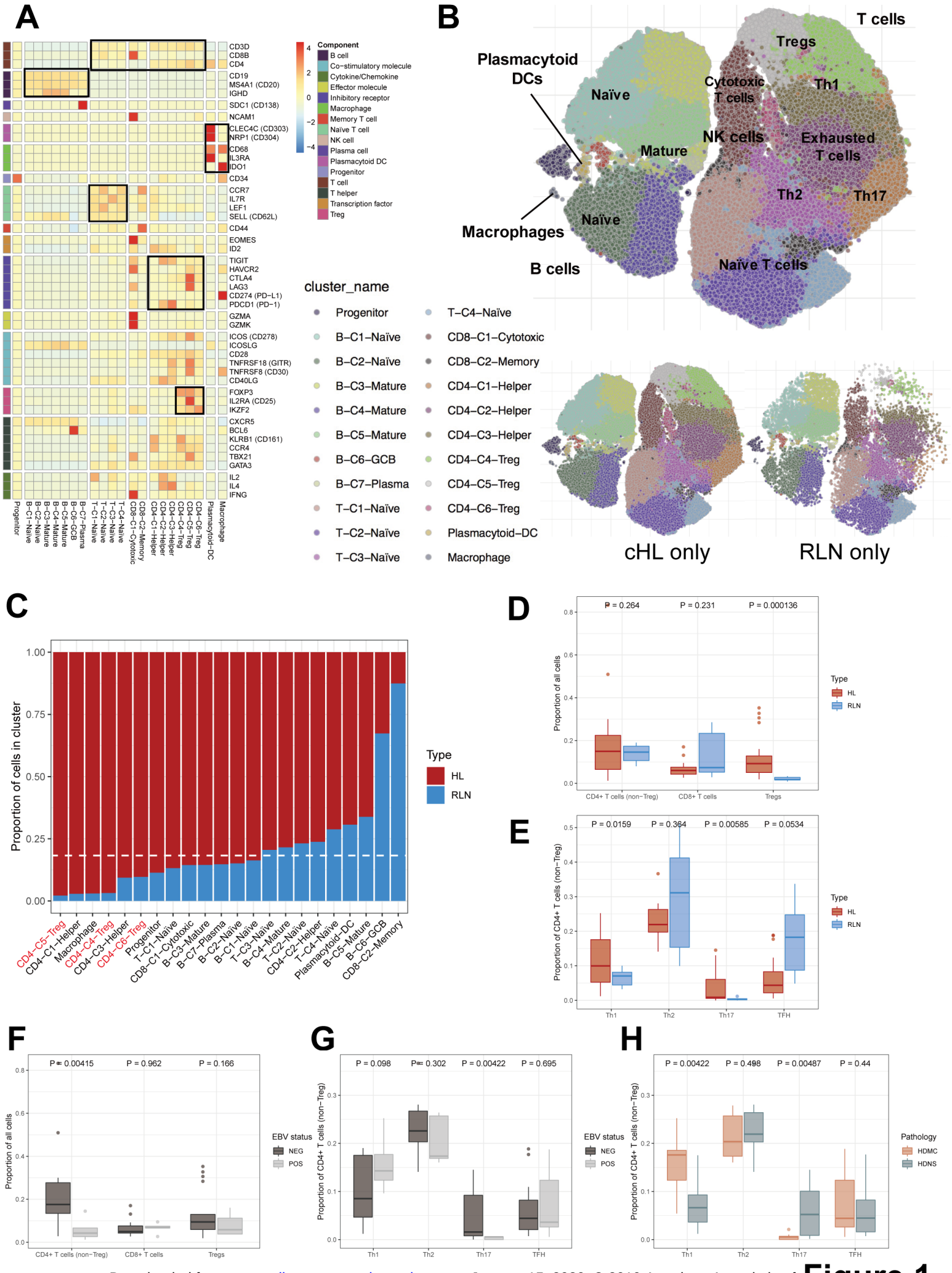

Figure 1

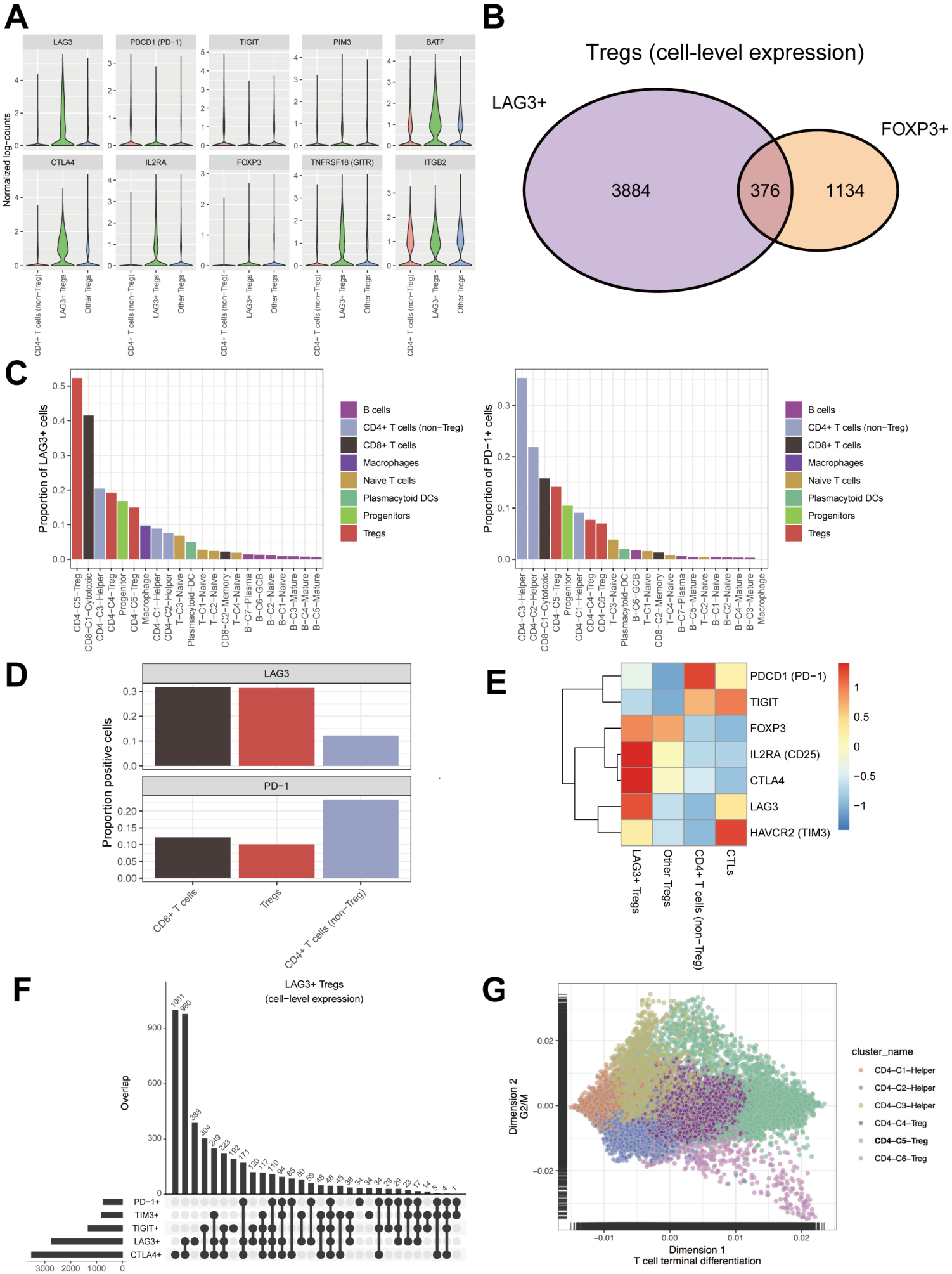

Figure 2

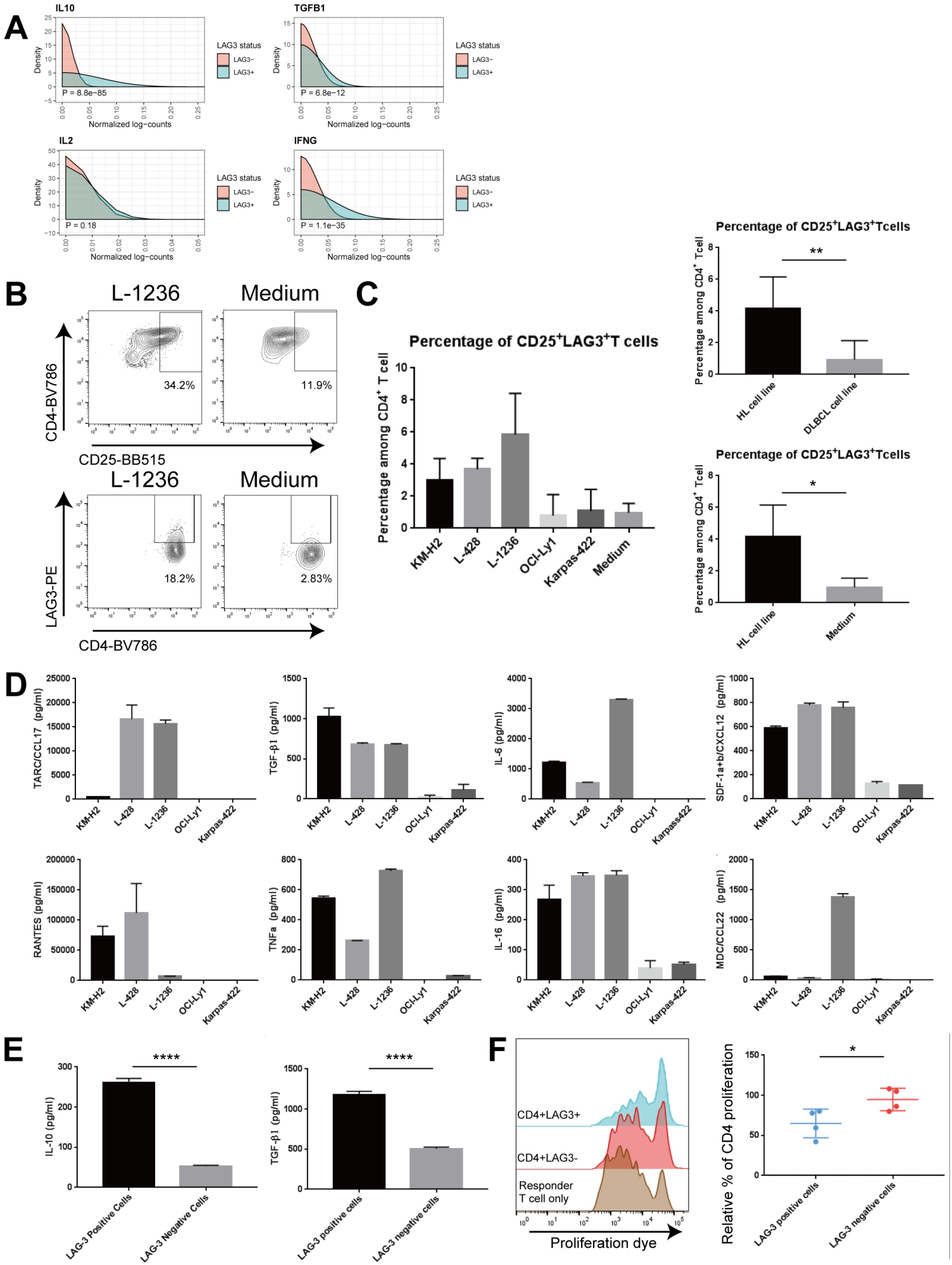

Figure 3

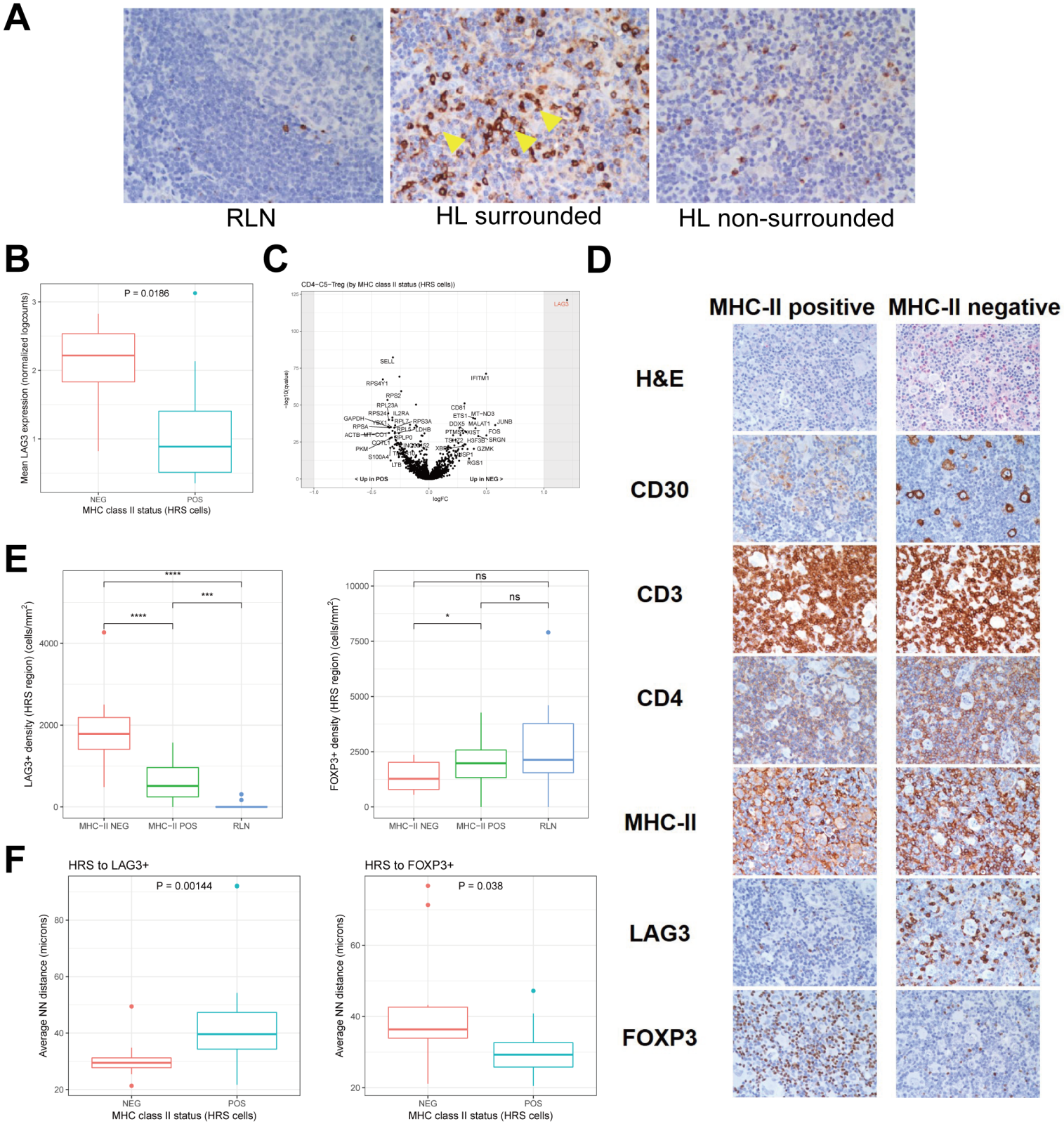

Figure 4

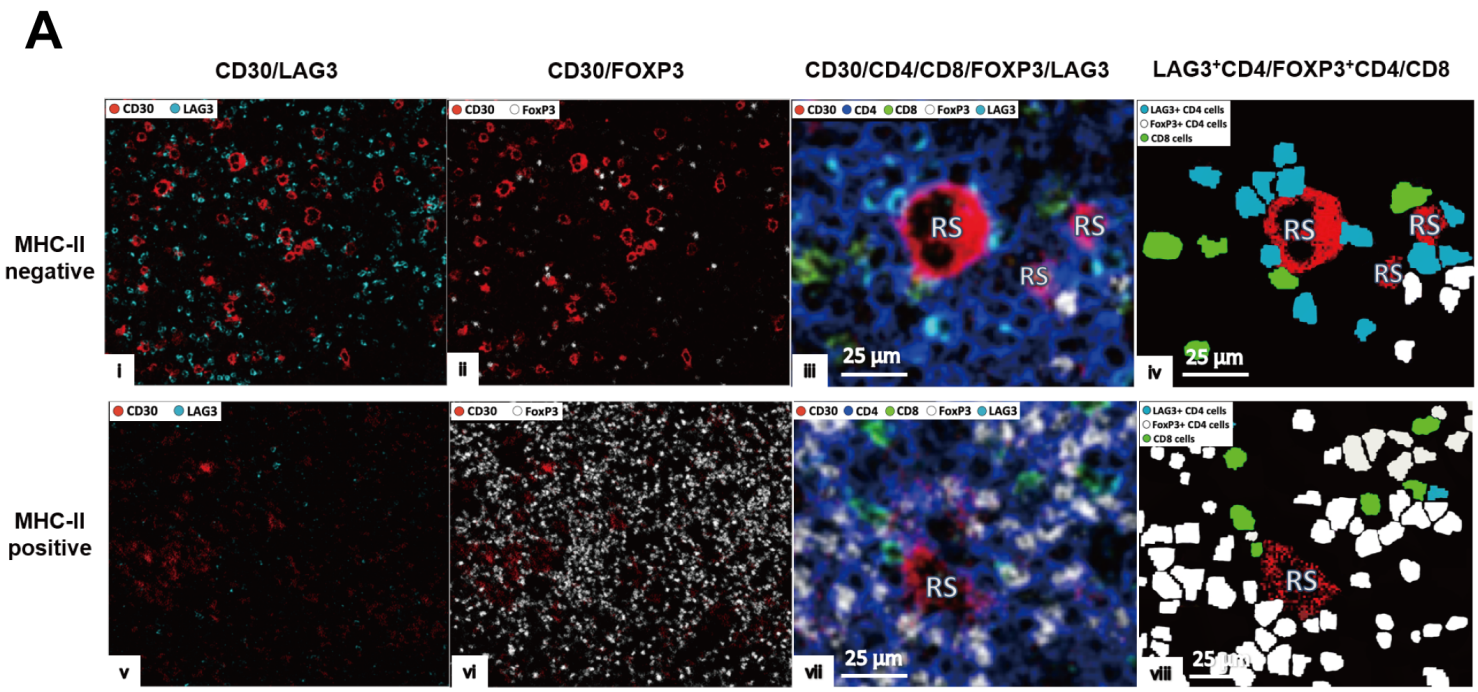

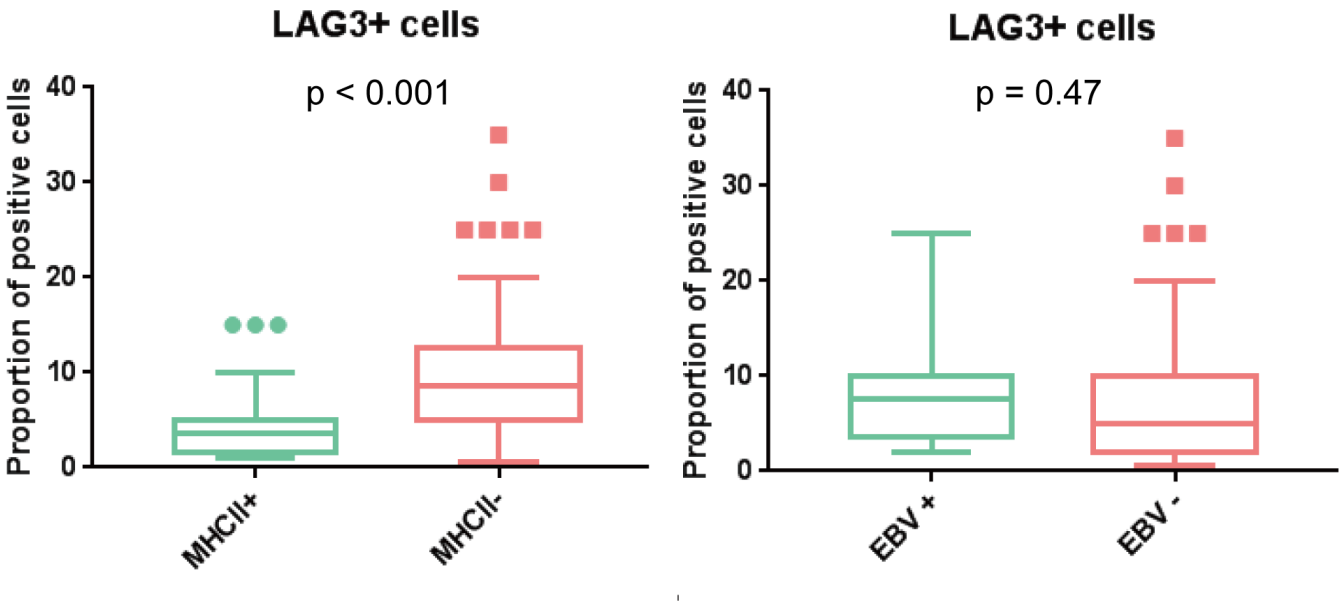

Figure 5

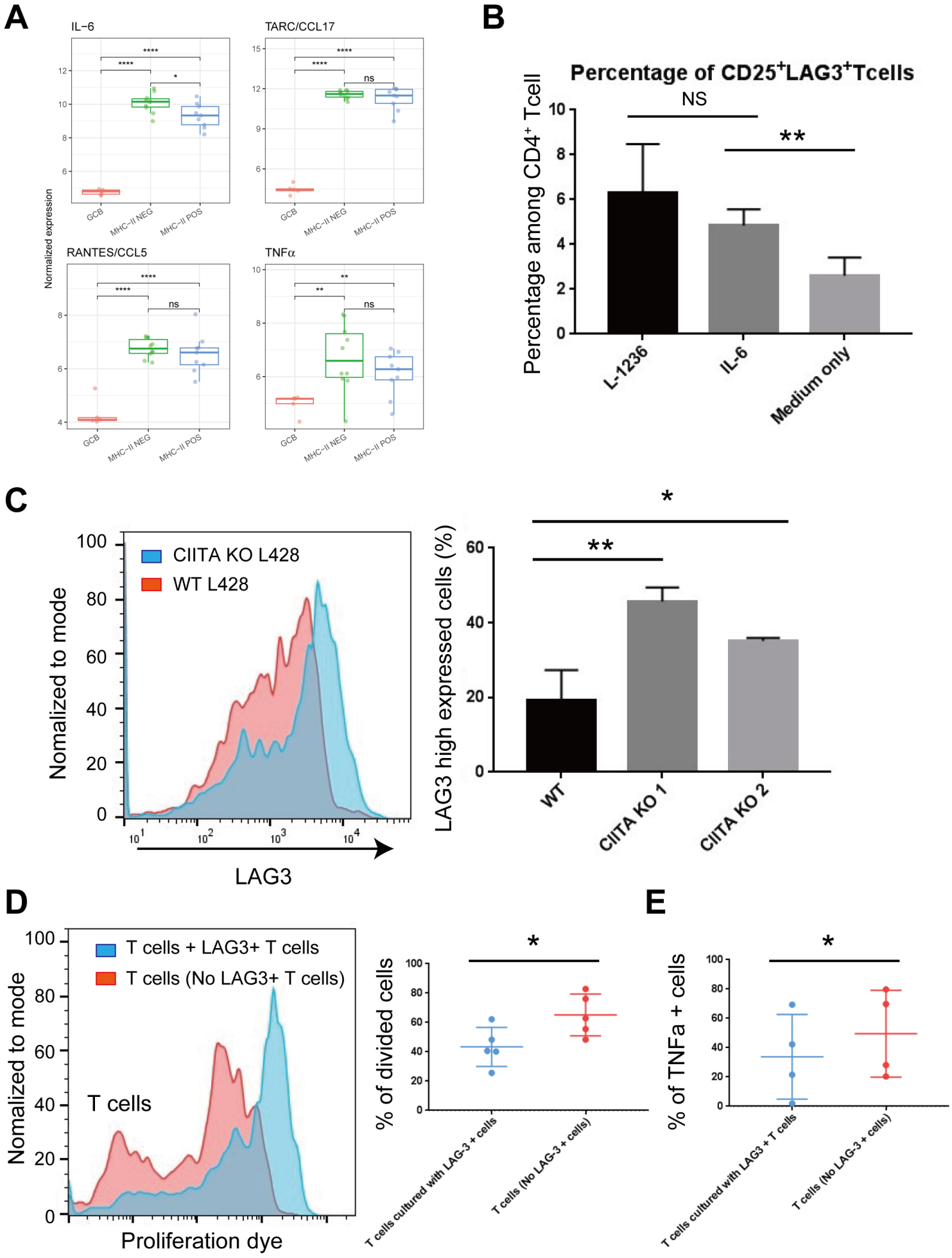

Figure 6

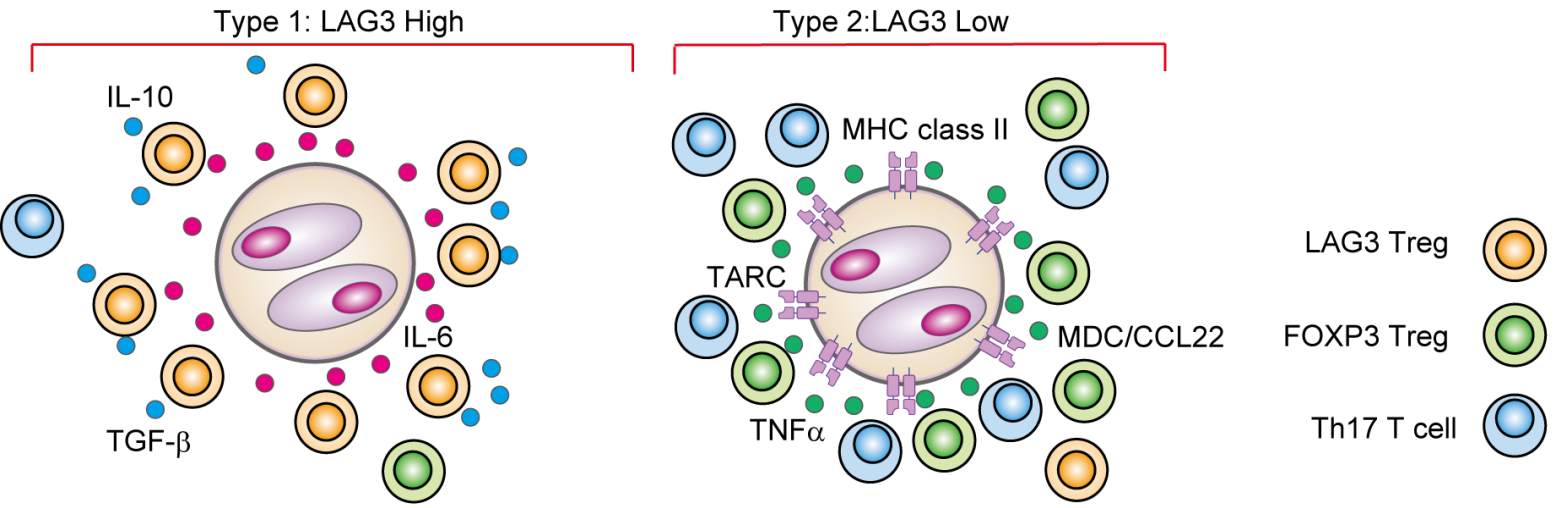

Figure 7

AACR American Association for Cancer Research

CANCER DISCOVERY

Single cell transcriptome analysis reveals disease-defining T cell subsets in the tumor microenvironment of classic Hodgkin lymphoma

Tomohiro Aoki, Lauren C Chong, Katsuyoshi Takata, et al.

Cancer Discov Published OnlineFirst December 19, 2019.